



ELSEVIER

Available online at www.sciencedirect.com

SCIENCE @ DIRECT®

International Journal of Solids and Structures 43 (2006) 1727–1745

INTERNATIONAL JOURNAL OF
**SOLIDS and
STRUCTURES**

www.elsevier.com/locate/ijsolstr

Dual-indentation technique for the assessment of strength properties of cohesive-frictional materials

F.P. Ganneau, G. Constantinides, F.-J. Ulm *

Massachusetts Institute of Technology, CEE-1 263, 77 Mass Ave, Cambridge, MA 02139, USA

Received 30 November 2004; received in revised form 9 March 2005

Available online 18 April 2005

Abstract

We propose a dual indentation technique for the assessment of the cohesion and friction angle of cohesive-frictional materials of the Mohr–Coulomb type. The technique is based on a computational implementation of the yield design theorems applied to conical indentation tests with different apex angles. The upper bound solutions are found to be very close to flat indentation solutions available for cohesive-frictional materials. On this basis we derive fundamental hardness-to-cohesion solutions in function of the friction angle and the apex angle. By studying the property of these dimensionless relations, we show that the ratio of two hardness measurements obtained from indentation tests with different apex angles, allows one to determine the friction angle. This dual indentation method is applied to Berkovich and Corner Cube indenter assimilated to equivalent cones of different apex angle. The method is validated for a ‘model’ material, metallic glass, which has recently been identified as a cohesive-frictional materials. The only input to the method are two hardness values which we obtain by microindentation on metallic glass. The outcome are values of the cohesion and friction angle, which are found to be in excellent agreement with reported cohesion and friction angle values of metallic glass obtained by macroscopic triaxial testing and comprehensive finite-element backanalysis of indentation curves.

© 2005 Elsevier Ltd. All rights reserved.

Keywords: Indentation analysis; Hardness; Cohesive-frictional materials; Yield design solution; Dual indentation technique

* Corresponding author. Tel.: +1 617 253 3544; fax: +1 617 253 6044.
E-mail address: ulm@mit.edu (F.-J. Ulm).

1. Introduction

The hardness of materials is a fundamental quantity used in Materials Science and Engineering for materials property characterization. It is obtained in a standardized fashion from an indentation test by dividing the applied load P by the area of the contact surface projected on the initial sample surface, A_c (see for instance Borodich and Keer, 2004):

$$H \stackrel{\text{def}}{=} \frac{P}{A_c}. \quad (1)$$

From the very beginning of hardness measurements of metals (Brinell, 1901; Williams, 1942; Tabor, 1951), the hardness was found to correlate with strength properties. From slip-line field solution for indentation in a rigid-plastic solids by a frictionless rigid wedge, Tabor (1948) suggested a hardness vs. yield stress relationship of the form $H/Y = 3$. This ‘rule of thumb’ (Schuh and Nieh, 2004) got under scrutiny by several researchers for conical indentation into rigid plastic solids with and without contact friction (Locket, 1963; Chitkara and Butt, 1992), elastic-perfectly plastic solids (see discussion in Johnson, 1985) and more recently for work-hardening materials (Cheng and Cheng, 2004). All these studies lead to the conclusion that hardness is not a material property, but rather a snapshot of materials mechanical properties and indenter geometry dependent. This conclusion does not only hold for cohesive materials (of the Von-Mises or Tresca-type), but as well for cohesive-frictional materials: several researchers report hardness-to-compressive strength ratios for frictional materials on the order of $H/Y_c \simeq 20\text{--}30$ (Kholmyansky et al., 1994; Igarashi et al., 1996; Constantinides et al., 2003), which highlights the effect of internal friction on the hardness of cohesive-frictional materials. But in contrast to cohesive materials, the hardness-strength relation for indentation in cohesive-frictional materials has not been studied in the same depth, and is the focus of this paper.

To motivate the forthcoming developments, consider a conical indentation test on a homogeneous elastic perfectly plastic cohesive-frictional material half-space. The two dependent quantities of interest that define the hardness, force P and contact area A_c , depend on the material properties (stiffness C_{ijkl} , cohesion c , friction angle φ), the indentation geometry (which in the case of conical indentation reduces to the half-apex angle θ), and the indentation depth h :

$$P = f(C_{ijkl}, c, \varphi, \theta, h), \quad (2a)$$

$$A_c = g(C_{ijkl}, c, \varphi, \theta, h). \quad (2b)$$

From a straightforward application of dimensional analysis (or more precisely the Pi-Theorem) to relations (2), it is readily found that the two dimensionless relations,

$$\frac{P}{ch^2} = \Pi_\alpha \left(\frac{C_{ijkl}}{c}, \varphi, \theta \right), \quad (3a)$$

$$\frac{A_c}{h^2} = \Pi_\beta \left(\frac{C_{ijkl}}{c}, \varphi, \theta \right), \quad (3b)$$

define a unique third dimensionless relation, the hardness-to-cohesion ratio as a unique function of the stiffness-to-cohesion ratio, the friction angle and the half-apex angle θ :

$$\frac{H}{c} = \frac{\Pi_\alpha}{\Pi_\beta} = \mathcal{H}_c \left(\frac{C_{ijkl}}{c}, \varphi, \theta \right). \quad (4)$$

Relation (4) has been extensively studied for elasto-plastic cohesive materials ($\varphi = 0$), with and without strain hardening (see review in Cheng and Cheng, 2004). In particular, it has been shown, that the H/c –

ratio for cohesive materials, for which $(C_{ijkl}/c)^{-1} \rightarrow 0$, comes close to Tabor’s suggestion (noting that $Y = 2c$ for a Tresca material):

$$\frac{H}{Y} = \frac{H}{2c} = \frac{1}{2} \mathcal{H}_c \left(\frac{C_{ijkl}}{c} \rightarrow \infty, \varphi = 0, \theta \right) \simeq 2.8 \tag{5}$$

A similar limit analysis result is still missing for conical indentation in cohesive-frictional materials, since—as Johnson (1985) notes in his classical book—‘problems of axi-symmetrical plastic flow cannot, in general, be solved by the method of characteristics (slip lines) as in plane strain (page 168)’. Indeed, to our knowledge, the only analytical slip-line solutions we found for cohesive-frictional materials in axi-symmetrical conditions are for flat punch indentation problems (the circular foundation problem), for which $\theta = \pi/2$ (Hopkins et al., 1961; Salençon and Matar, 1982). Of course, like for pure cohesive materials, the finite-element method has been employed for the inverse analysis of indentation load *vs.* indentation depth curves for some particular cohesive-frictional materials, such as metallic glass (Vaidyanathan et al., 2001). Beside questions concerning the uniqueness of this inverse problem (Cheng and Cheng, 2004), finite element analysis are computational too intensive to be used for day-to-day applications in instrumented indentation analysis. Hence, a solution for conical indentation is highly desirable as a first engineering approach to the assessment of the cohesion and friction angle of cohesive-frictional materials. This is the focus of this paper. By means of an original computational implementation of the limit theorems of yield design, we develop such a solution, of the form:

$$\frac{H}{c} = \mathcal{H}_c(\varphi, \theta). \tag{6}$$

2. Yield design approach for conical indentation

2.1. Problem formulation

Consider an indentation test of a rigid conical indenter into an infinite half-space oriented in the $-z$ direction (Fig. 1). The indenter is at an indentation depth h , the projected contact area A_c is assumed to be known, and a force P is applied. The work rate provided from the outside to the (half-space materials) system is:

$$\delta W = P \dot{h} = \int_{AM} \underline{T}(\underline{n}) \cdot \underline{U} da, \tag{7}$$

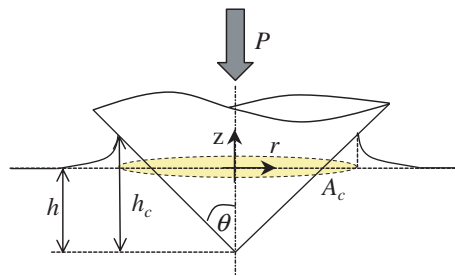


Fig. 1. Conical indentation test: h is the indentation depth; h_c is the contact height; A_c is the contact surface projected on the initial sample surface.

where \dot{h} is the rate of indentation depth, $A_M = A_c / \sin \theta$ is the contact area of the cone mantle with the material (A_c being the projection of this surface on the z -axis); $\underline{T}(\underline{n}) = \underline{\sigma} \cdot \underline{n}$ is the stress vector on A_M oriented by the unit outward normal \underline{n} (positive outward to the material domain; i.e. in a cylinder coordinate frame $\underline{n} = -\cos \theta \underline{e}_r + \sin \theta \underline{e}_z$); and \underline{U} is the velocity field of the material on A_M .

In elastoplastic problems, a part of the external work rate (7) is stored into recoverable elastic energy (incl. hardening) into the material system. By contrast, limit analysis is based on the assumption, that a materials system, at plastic collapse, has exhausted, in response to the prescribed force P , its capacities, (i) to develop stress fields that are both statically compatible (i.e. in equilibrium) with the external loading and compatible with the local strength domain of the constitutive materials; and (ii) to store the externally supplied work rate (7) into recoverable elastic energy. As a consequence, the work rate δW is entirely dissipated in the material bulk and along surfaces of discontinuity; hence from an application of the generalized divergence theorem to (7):

$$\delta W = \int_{\Omega} \pi(\mathbf{d}) \, d\Omega + \int_{\Gamma} \pi([\underline{U}]) \, d\Gamma, \quad (8)$$

where $\pi(\mathbf{d}) = \sup \underline{\sigma} : \mathbf{d}$ and $\pi([\underline{U}]) = \sup \underline{T} \cdot [\underline{U}]$ is the maximum dissipation capacity the material can develop in the material bulk and along surfaces of discontinuity for the solution fields $(\underline{\sigma}, \underline{U})$. The solution stress field $\underline{\sigma}$ is statically and plastically admissible, satisfying:

$$\underline{\sigma} = {}^t \underline{\sigma}; \quad \text{div} \underline{\sigma} = 0; \quad [[\underline{T}]] = [[\underline{\sigma} \cdot \underline{n}]] = 0, \quad (9a)$$

$$f(\underline{\sigma}) \leq 0; \quad f(\underline{T}) \leq 0, \quad (9b)$$

where superscript t stands for transpose; and $f(\underline{\sigma})$ and $f(\underline{T})$ are the yield function defining the strength domain of the material system respectively in continuous material sub-domains and on surfaces of discontinuity; while \mathbf{d} is the solution strain rate field in continuous material sub-domains, and $[[\underline{U}]]$ is the velocity jump over surfaces of discontinuity Γ , which are kinematically compatible with the velocity field \underline{U} , and compatible with the plastic flow rule of the material:

$$\mathbf{d} = \frac{1}{2} (\text{grad} \underline{U} + {}^t \text{grad} \underline{U}) = \lambda \frac{\partial f}{\partial \underline{\sigma}} \quad (10a)$$

$$[[\underline{U}]] = \underline{U}^+ - \underline{U}^- = \lambda \frac{\partial f}{\partial \underline{T}} \quad (10b)$$

Provided that $(\underline{\sigma}, \underline{U})$ are related through (10) by the normality rule of plastic flow, the dissipation functions are unique functions of the strain rate (respectively velocity jump) only. For instance, for a Mohr–Coulomb material, for which the yield function is given by:

$$f(\underline{\sigma}) = \sigma_I (1 + \sin \varphi) - \sigma_{III} (1 - \sin \varphi) - 2c \cos \varphi \leq 0, \quad (11a)$$

$$f(\underline{T}) = |{}^t \underline{T} \cdot \underline{T}(\underline{n})| + \tan \varphi (\underline{n} \cdot \underline{T}(\underline{n})) - c \leq 0, \quad (11b)$$

the volume dissipation functions reads (Salençon, 1983):

$$\pi(\mathbf{d}) = \begin{cases} \rho \text{tr} \mathbf{d} & \text{if } \text{tr} \mathbf{d} \geq \sin \varphi (|d_I| + |d_{II}| + |d_{III}|) \\ +\infty & \text{else} \end{cases} \quad (12)$$

and the discontinuity dissipation function:

$$\pi([\underline{U}]) = \begin{cases} c |U_t| & \text{if } U_n \geq |U_t| \tan \varphi \\ +\infty & \text{else} \end{cases}, \quad (13)$$

where $\sigma_I \geq \sigma_{II} \geq \sigma_{III}$ are principal stresses; $d_I \geq d_{II} \geq d_{III}$ are principal strain rates; $U_t = \underline{t} \cdot [[\underline{U}]]$ and $U_n = \underline{n} \cdot [[\underline{U}]]$ are respectively the tangential and normal velocity jump, and $\rho = c \cot \varphi$ is the cohesive pressure.

The limit theorems of yield design approach the actual dissipation capacity (8) by a lower and an upper bound estimate. The lower estimate is based on statically and plastically admissible stress fields σ' and stress vectors \underline{T}' satisfying (9); and the upper bound approach on kinematically and plastically admissible strain rate fields \mathbf{d}' and velocity jumps $[[\underline{U}']]$, satisfying (10). Noting that $\text{tr } \mathbf{d}' = \text{div } \underline{U}'$ in (12) and making use of the generalized divergence theorem for the upper bound, the limit theorems for the conical indentation problem into a homogeneous Mohr–Coulomb material half-space can be written in the form:

$$-\int_{A_M} \underline{T}'(\underline{n}) \cdot \underline{e}_z \, da \leq P \dot{h} \leq \rho \int_{\partial\Omega} \underline{U}' \cdot \underline{n} \, da. \tag{14}$$

Herein, $P' = -\int_{A_M} \underline{T}'(\underline{n}) \cdot \underline{e}_z \, da$ is a lower bound limit indentation load in equilibrium with statically and plastically admissible stress fields σ' in Ω , satisfying (9) and (12) while $\underline{U}' \cdot \underline{n}$ is the normal component of the velocity field at the surface $\partial\Omega$ of the half-space, which includes the cone mantel A_M oriented by $\underline{n} = -\cos \theta \underline{e}_r + \sin \theta \underline{e}_z$, and the stress-free surface outside the contact radius $r \geq r_c = \sqrt{A_c/\pi}$. In order for the dissipation to remain finite, this surface velocity field \underline{U}' must be such to locally satisfy the inequalities in (12) and (13). Finally, since the contact area A_c is assumed to be known, inequalities (14) can be recast in the form of the dimensionless relation (6):

$$\frac{H^-}{c} \leq \frac{H}{c} = \mathcal{H}_c(\varphi, \theta) \leq \frac{H^+}{c} = \frac{\delta'(\varphi, \theta)}{\tan \varphi}, \tag{15}$$

where $\delta'(\varphi, \theta) = \frac{1}{A_c} \int_{\partial\Omega} \underline{U}' \cdot \underline{n} \, da$ (with $\overline{\underline{U}'} = \underline{U}'/\dot{h}$ the normalized surface velocity field) can be seen as a global dilatation coefficient. Hence, any statically admissible stress-strength solution provides a lower bound H^-/c to the sought dimensionless relation (6) and for any velocity-flow rule solution it is the inverse.

Last, for either lower and upper bound, we need to define boundary conditions, or more precisely contact conditions at the indenter–material interface. For a frictionless contact condition, all shear stresses at the interface are zero, i.e. $\forall \underline{t} \cdot \underline{n} = 0; \underline{t} \cdot \underline{T}'(\underline{n}) = 0 \iff \underline{T}'(\underline{n}) = \sigma' \underline{n}$:

$$\forall (r, z) \in A_M; \begin{cases} \underline{t} \cdot \underline{T}'(\underline{n}) = \frac{1}{2}(\sigma'_{zz} - \sigma'_{rr}) \sin 2\theta + \sigma'_{rz} \cos 2\theta = 0 \\ \underline{n} \cdot \underline{T}'(\underline{n}) = \sigma'_{rr} \sin^2 \theta + \sigma'_{zz} \cos^2 \theta - \sigma'_{rz} \sin 2\theta \end{cases} \tag{16}$$

$$\forall r \geq r_c; \quad z = 0 : \underline{T}'(\underline{n}) = 0.$$

In the upper bound approach, a velocity field is kinematically admissible, if it satisfies the zero-velocity boundary conditions at infinity. On the other hand, there is an additional interface condition, which arises from a frictionless contact condition, which a priori permits a tangential slip (without dissipation), while the normal velocity $\underline{U}' \cdot \underline{n}$ is the one of the rigid indenter:

$$\forall (r, z) \in A_M; \quad \underline{U}' \cdot \underline{n} = -\dot{h} \sin \theta, \tag{17}$$

$$(r, z) \rightarrow \infty; \quad \underline{U}' = 0.$$

2.2. Formulation as optimization problem

The limit theorems define two formidable optimization problems, either to construct statically admissible stress fields σ' that maximize the indentation load (respectively the hardness); or to construct kinematically admissible velocity fields \underline{U}' that minimize the maximum dissipation capacity the material can support. Given the limited possibilities for analytical solutions (such as slip-line solutions), the beneficial

use of a continuum discretization into finite elements together with linear programming techniques was early on recognized for the implementation of both the lower bound theorem for plane-stress conditions (Lysmer, 1970; Pastor, 1976; Pastor and Turgeman, 1976) and the upper bound theorem for plane-strain conditions (Anderheggen and Knopfel, 1972; Fremond and Salençon, 1973; Turgeman, 1976; Bottero et al., 1980). The most advanced implementation is due to Sloan and co-worker combining (plane stress/plane strain) 2-D or 3-D linear finite element formulations with linear and non-linear programming (Sloan, 1988a, ; Sloan and Kleeman, 1995; Lyamin and Sloan, 2002a,b). We employ a similar strategy for the axi-symmetrical conditions of the indentation test, which to our knowledge have not been addressed in the open literature. The material domain is discretized by linear finite elements (triangles in 2-D, tetrahedra in 3-D). In the lower bound approach, stress discontinuities are a priori permitted for out of-plane stresses provided that the stress vector continuity ($[[\sigma' \cdot \underline{n}]] = 0$) is enforced as a constraint condition over common edges of adjacent elements. This is achieved by designing nodes to elements, so that multiple nodes share the same set of coordinates. A similar strategy is employed to model velocity jumps in the upper bound approach.

In the lower bound approach, the stress field is discretized in the form:

$$\sigma'_{ij} = \sum_k N_k(r, z) \sigma_{ij}^k, \quad (18)$$

where σ_{ij}^k are the nodal stresses and N_k are linear shape functions which in axi-symmetrical conditions depends only on r, z . Since most optimization algorithms come as minimization algorithm, the lower bound optimization problem for the indentation test is formulated using as objective function $\max_{\sigma_{ij}^k}(H^-) = \min_{\sigma_{ij}^k}(-H^-)$ in the discretized form for a unit projected contact area:

$$\left\{ \begin{array}{l} -H^- = -\min_{\sigma_{ij}^k} [C]^T [\sigma'] \\ \text{Subject to:} \\ [A_1][\sigma'] - [b_1] = 0 \\ F(\sigma') \simeq [A_2][\sigma'] - [b_2] \leq 0 \end{array} \right\}. \quad (19)$$

Herein, $[C]$ assembles the objective function matrices for the nodes along the cone surface from a discretization of the lower bound integral in (14); $[A_1]$ and $[b_1]$ assemble the constraint coefficients arising from a discretization of the momentum balance $\text{div } \sigma' = 0$ per element, of the stress vector continuity $[[\sigma' \cdot \underline{n}]] = 0$ over shared edged of elements, and of extension elements at the boundary of the discretized domain, which extend the statically admissible stress field beyond the limits of the domain discretized by finite elements. $F(\sigma')$ assembles the constraints arising from the yield criterion (11a) at all nodes (including the one of the extension elements situated at the boundary), which ensures that the stress field is plastically admissible throughout the entire half-space. In order to satisfy the strength criterion (11b) throughout the element, it suffices to enforce it at the element nodes since the stresses vary linearly (Lyamin and Sloan, 2002a). This reduces the number of inequalities significantly. Furthermore, in order to employ the tools of linear programming (thus avoiding nonlinear constraints on the unknown nodal stresses), the Mohr–Coulomb criterion is linearized through a polygonal approximation of the principal stresses, which is expressed by the matrix $[A_2]$ and vector $[b_2]$ in (19). The derivation and expressions of the matrices and vectors for axi-symmetrical conditions can be found in Ganneau and Ulm (2004).

In the upper bound approach, the velocity field is discretized in the form:

$$U'_i = \sum_k N_k(r, z) u_i^k, \quad (20)$$

where u_i^k are the nodal velocities and N_k are linear shape functions. Using the classical notation of displacement-based finite element formulation (see e.g. Bathe, 1996) which is here applied to the velocity

formulation, the components of the strain rate tensor are given by $[d'] = [B_{ij}][u_i^k]$, where $[B_{ij}]$ is the strain rate–velocity matrix (equivalent to the strain–displacement matrix in the FEM), which allows a straightforward calculation of the maximum local dissipation capacity per element from (12) and along surfaces of discontinuities (i.e. joined edges between elements) from (13). Integrated over the discretized half-space domain, it is this dissipation capacity which is minimized in the upper bound implementation; i.e. formally:

$$\left\{ \begin{array}{l} H^+ = \min_{u_i^k} [C']^T [\bar{U}'] \\ \text{Subject to:} \\ [A'_1][\bar{U}'] - [b'_1] = 0 \\ G(\bar{U}') \simeq [A'_2][\bar{U}'] - [b'_2] \leq 0 \end{array} \right\}, \tag{21}$$

where $[\bar{U}'] = u_i^k / \dot{h}$ is the normalized nodal velocity vector and matrix $[C']$ assembles the (unit) element and discontinuity dissipation terms. The equality constraints arise from the contact condition (17), while $G(\bar{U}') \leq 0$ assembles the constraints arising from the conditions $g(\mathbf{d}') = \sin \varphi (|d'_{I'}| + |d'_{II'}| + |d'_{III'}|) - \text{tr} \mathbf{d}' \leq 0$ and $g([\bar{U}']) = |U_t| \tan \varphi - U_n \leq 0$ in (12) and (13), that ensure the finiteness of the (local) dissipation. In order to preserve the nature as a linear programming tool, these (nonlinear) inequality constraints were linearized (on similar lines as the Mohr–Coulomb criterion), in a series of linear inequalities. The derivations and expressions of the matrices and vectors can be found in Ganneau and Ulm (2004).

Finally, it should be noted that we evaluate both the lower and the upper bound theorem on an idealized geometrical indentation configuration, by considering the surface surrounding the indenter to be flat and not deformed. In other words, we neglect in the evaluation of the dissipation capacity sinking-in or piling-up phenomena in the immediate surrounding of the indenter. The error one commits through such an idealized geometrical configuration should be on the order of the sink-in or pile-up volume, which however should be of second order compared to the material bulk volume that contributes to the overall dissipation capacity.

2.3. Validation for flat punch problem

To validate our yield design solutions, we consider the flat punch problem, or rigid circular footing ($\theta = \pi/2$), on a Mohr–Coulomb half-space, for which two benchmark solutions within the framework of limit equilibrium theory in axi-symmetrical conditions are available. The first solution, which is due to Hopkins et al. (1961), is for the ‘smooth’ punch corresponding to the frictionless boundary conditions (16) and (17):

$$\forall (r, z = 0) \in A_M; \left\{ \begin{array}{l} \sigma' = -\sigma'_{zz}; \sigma'_{rz} = 0 \\ \underline{U}' \cdot \underline{n} = -\dot{h} \end{array} \right\}. \tag{22}$$

It is based on kinematically admissible velocity fields \underline{U}' , i.e. an upper bound approach, which is shown to be compatible with a statically and plastically admissible stress field $\sigma_{ij}^*(\underline{U}')$ in the bounded region below the footing and throughout the rest of the half-space satisfying the lower bound conditions (9). Hence, the slip-line solution for the smooth flat punch problem is the exact plastic collapse solution in the sense of relations (7), (8), (9) and (10). The second benchmark solution is due to Salençon and Matar (1982): a perfectly rough punch on a Mohr–Coulomb half-space. The perfectly rough punch translates into a frictional interface stress condition and a no-slip velocity condition of the form:

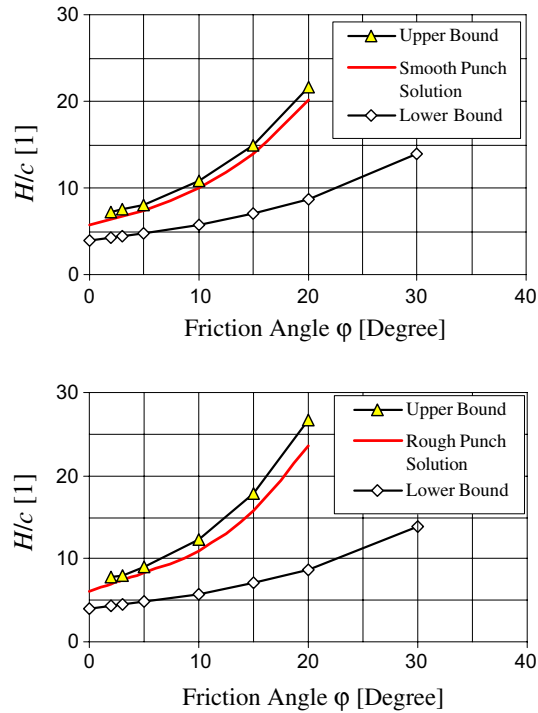


Fig. 2. Hardness-to-cohesion solutions for the flat punch problem: top: ‘Smooth’ punch solutions (benchmark solution of Hopkins et al., 1961); bottom: ‘Perfectly rough’ punch solutions (benchmark solution of Salençon and Matar, 1982).

$$\forall (r, z = 0) \in A_M; \left\{ \begin{array}{l} f'(\underline{T}') = |\sigma'_{rz}| + \tan \varphi \sigma'_{zz} - c \leq 0 \\ \underline{U}' \cdot \underline{n} = -\dot{h}; \underline{U}' \cdot \underline{t} = 0 \end{array} \right\}. \quad (23)$$

Matar and Salençon’s solution is based on statically and plastically admissible stress fields σ'_{ij} , *ie.* a lower bound approach, constructed by the method of characteristics along characteristic lines in a zone spreading under the foundation and emerging at the stress-free surface. In this same zone a velocity field $\underline{U}^*(\sigma'_{ij})$ is constructed that satisfies the compatibility conditions (10) and (23)₂; yielding a so-called ‘incomplete solution’ (Bishop, 1953), as the stress field and the velocity fields have not been extended throughout the rest of the half-space. Both solutions employ the Haar–Karman hypothesis¹ which is a posteriori verified.

Fig. 2 display the lower and upper bounds of the hardness-to-cohesion relation $H/c = \mathcal{H}_c(\varphi, \theta = \pi/2)$, we obtain with our algorithms for the smooth punch problem and the rough punch problem together with the benchmark solutions. The upper bound solution comes remarkably close to the exact solution of Hopkins et al. (1961), and also very close to the ‘incomplete’ (lower bound solution) of Salençon and Matar (1982) (the maximum relative difference is consistently less than 6%); while the lower bound solution

¹ The Haar–Karman hypothesis assumes that the middle principle stress is equal either to the major or minor principal stress,

$$\sigma_{II} = \frac{1}{2}[(\sigma_I + \sigma_{III}) - \epsilon(\sigma_I - \sigma_{III})]; \quad \epsilon = \pm 1.$$

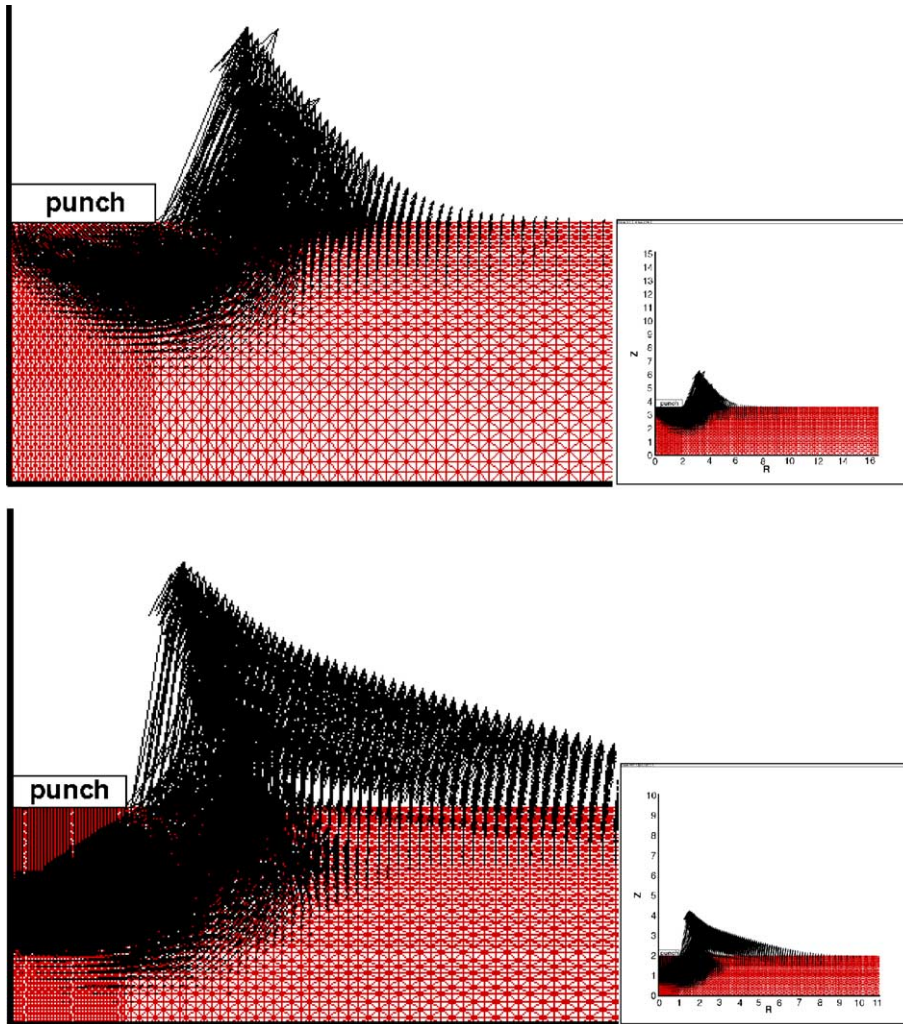


Fig. 3. Velocity fields for the upper bound flat punch solutions: top: frictionless indenter–material interface condition, bottom: perfectly rough interface ($\varphi = 10^\circ$).

perform rather poorly. The reason for this poor performance is that the algorithm converges towards diagonal stress fields (no shear stress) due to the stress-free boundary condition on $r \geq r_c$, which propagates $\sigma'_{rz} = 0$ from the surface boundary into the entire domain (Ganneau and Ulm, 2004). Because of this restriction to diagonal stress fields, the lower bound approach is limited to a relative small range of possible stress solutions that appear too restrictive to come close to the actual stress fields in the punch tests. In contrast, the upper bound approach is free of such restrictions and is able to accommodate any collapse mechanism (see Fig. 3), converging towards the actual dissipation capacity. The observation that the upper bound solutions appear much more realistic than the lower bound solutions does not only hold for the punch problem, but was verified for all types of axi-symmetrical indentation tests: conical, spherical, etc. (for details, see Ganneau and Ulm, 2004). This and the excellent agreement of the flat punch solutions with the reference solutions are very strong arguments in favor of the use of the upper bound solution for indentation analysis.

3. Dual indentation approach

In this section, we develop a dual indentation approach for the assessment of cohesion and friction angle of cohesive-frictional materials, which is based on the self-similarity of the conical indentation test, and on the dependence of the hardness-to-cohesion ratio (6) on two parameters only, the friction angle φ and the tip half-angle θ . We show that the approach satisfies the uniqueness of the inverse analysis to extract the strength properties of cohesive-frictional materials from two hardness measurements carried out with conical indenters of different apex angle. The dual indentation strategy we develop is of the same vain as other multiple indenter approaches recently proposed for elasto-plastic cohesive materials (with or without strain hardening) using conical or pyramidal indenters (Futakawa et al., 2001; Bucaille et al., 2003; Chollacoop et al., 2003; DiCarlo et al., 2003; Swaddiwudhipong et al., 2005), which all aim at overcoming the non-uniqueness of the reverse analysis of material properties from a single indentation test (Futakawa et al., 2001; Cheng and Cheng, 2004).

3.1. Hardness-to-cohesion relations for varying apex angles (at constant friction angle)

We ran upper-bound simulations for different tip apex angles (and frictionless contact conditions), while keeping the friction angle constant. Some results are displayed in Figs. 4 and 5 in form of a plot of H/c vs. θ (Fig. 4), together with some velocity fields for selected apex angles (Fig. 5). The resulting $H/c = \mathcal{H}(\varphi_0 = \text{const}, \theta)$ curve has a minimum around $\theta \simeq 45^\circ$ and increases for both smaller and larger apex angles. The increase for larger apex angles comforts the simple idea that a sharp cone ($\theta \geq 45^\circ$) is easier to drive into a material half-space than a flat punch ($\theta = 90^\circ$). This is evidenced from the velocity profiles shown in Fig. 5: the velocity profiles appear more concentrated for smaller apex angle than for larger apex angle. Hence, at plastic collapse, the amount of activated material volume that contributes to the overall dissipation decreases when the apex angle is reduced and reaches a minimum around $\theta \simeq 45^\circ$. Surprisingly, for very sharp cones ($\theta \leq 45^\circ$) there is an inverse trend, an apparent increase of the hardness, which may be due to the fact that the plastic zone concentrates into a material cone around the very sharp indenter whose volume increases quadratically compared to the volume of the conical indenter. A similar minimum phenomenon was reported by Houlsby and Wroth (1982) for the cone penetration test used in geotechnical

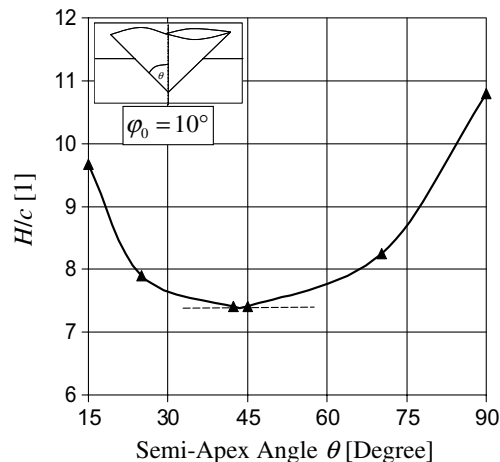


Fig. 4. Influence of the apex angle on the hardness-to-cohesion ratio ($\varphi = 10^\circ$). Evidence of the existence of a minimum.

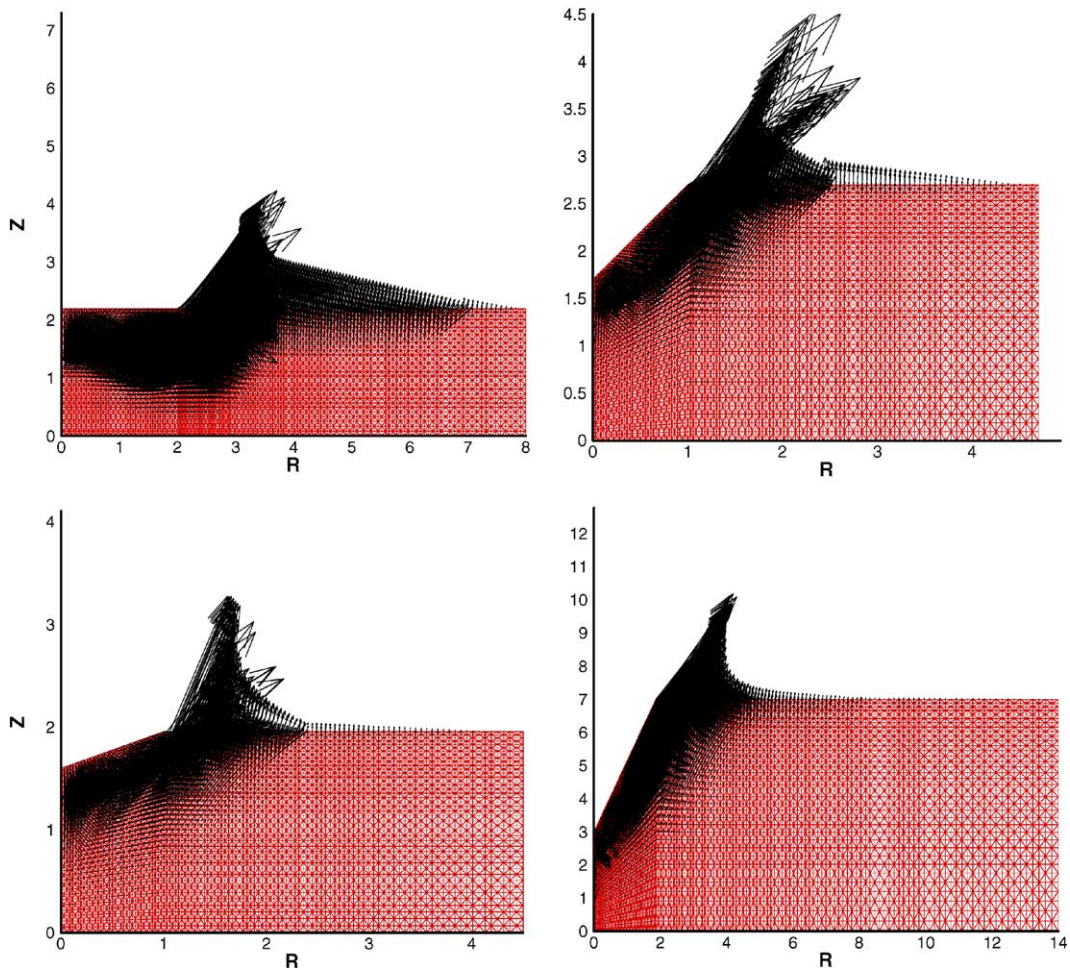


Fig. 5. Velocity fields for upper bound conical indentation solutions: (top-down, left-right) $\theta = 0^\circ$, $\theta = 70^\circ$, $\theta = 45^\circ$, $\theta = 25^\circ$ (all results for $\varphi = 10^\circ$).

applications, who reported a minimum of $\theta \simeq 50^\circ$ from exploring a lower bound approach. Such a minimum phenomenon has been also found for frictionless materials around $\theta \simeq 20^\circ$ (Chitkara and Butt, 1992), and the presence of friction appears to shift the minimum to higher cone angles. This minimum phenomenon is an important property regarding uniqueness of the inverse problem of the assessment of the cohesion and friction angle by two indentation tests. Indeed, provided that H/c , for a given friction angle, is a monotonic increasing (or decreasing) function of the apex angle, the uniqueness of the dual indentation method can be ensured.

3.2. Application to Berkovich and Corner cube indentation

By way of application, we consider two commercially available indenters that are commonly employed in instrumented indentation tests, the 3-sided pyramidal Berkovich and Cube Corner indenter. As it is common practice in indentation analysis (see e.g. Min et al., 2004), the 3-sided pyramids are assimilated to

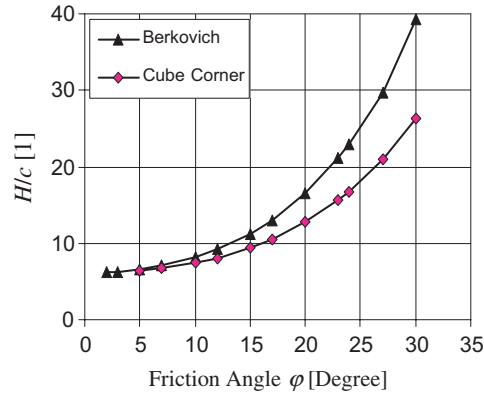


Fig. 6. Upper bound solutions for the hardness-to-cohesion ratio for two (equivalent conical) indenter geometries: Berkovich indenter ($\theta_B = 70.32^\circ$) and Cube Corner indenter ($\theta_{CC} = 42.28^\circ$).

cones so that the normalized projected contact area A_c/h^2 of the cone is the same as that of the real indenter, i.e. $A_c/h^2 = \pi \tan^2 \theta$. In the light of the results displayed in Fig. 4, it is readily understood that the effective cone angle of $\theta_B = 70.32^\circ$ for the Berkovich indenter and $\theta_{CC} = 42.28^\circ$ for the Cube Corner indenter ensure the uniqueness of the reverse problem. Fig. 6 displays the H^+/c – relations we determined with the upper bound approach for those two apex angles. Following the dimensionless expression (15), we fit the obtained results in a power-series of the form:

$$\frac{H^+}{c} = \frac{\delta'(\varphi, \theta)}{\tan \varphi} = \frac{1}{\tan \varphi} \sum_{k=1}^{k=N} (a_k(\theta) \tan \varphi)^k, \quad (24)$$

where coefficients $a_k(\theta)$ depend only on the apex angle. In the interval $\varphi \in [3^\circ, 30^\circ]$, a $N = 6$ power expression (i.e. fifth-order in $\tan \varphi$) fits perfectly the results, and the coefficients $a_k(\theta_B)$ and $a_k(\theta_{CC})$ are given in Table 1. While this fitting function is strictly valid only in the interval for which it was fitted, it may serve for limited extrapolation to higher friction angle. We ran simulations for $\varphi = 35^\circ$ and the results lay within the range of 1% from the fitted values. We should also note that the algorithm did not converge for a zero friction angle, since the implemented dissipation function of the Mohr–Coulomb (12) does not converge in a continuous fashion towards the dissipation function of the Tresca material ($\pi(d) = c(|d_I| + |d_{II}| + |d_{III}|)$), but becomes infinite for $\varphi = 0$. Hence, expression (24) with the fitted coefficients $a_k(\theta)$ of Table 1, has limited extrapolation capacity for frictionless materials. On the other hand, as the friction angle increases (for which our solution provide reliable results), we observe a strong deviation from the ‘rule-of-thumb’ value (5), generally admitted for metallic materials. In fact, internal friction kinematically impedes the 45° slip lines commonly observed for frictionless materials. As a consequence, the plastic yield volume increases

Table 1

Coefficients of power-series fit (24) for H/c relations of Berkovich indenter (θ_B) and Cube Corner indenter (θ_{CC}) assimilated to equivalent cones of same projected contact area

	a_1	a_2	a_3	a_4	a_5	a_6
$\theta_B = 70.32^\circ$	5.7946	2.9455	−2.6309	4.2903	−3.4887	2.7336
$\theta_{CC} = 42.28^\circ$	5.9455	2.4253	−2.7578	4.0152	−3.2938	2.5369

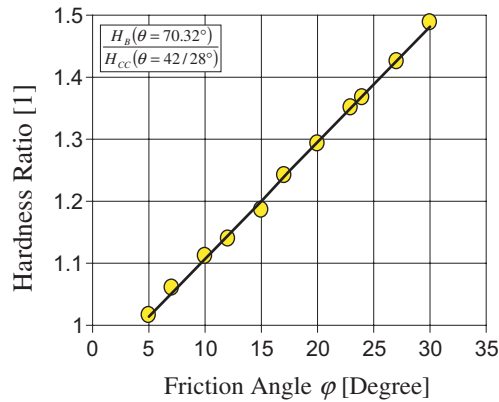


Fig. 7. Hardness-ratio (Berkovich/Cube Corner) vs. friction angle.

and thus the overall dissipation capacity of the system, which translates into a higher hardness value, and which is captured by the results displayed in Fig. 6.

On this basis, we can develop the dual indentation technique from a combination of Berkovich and Cube Corner hardness values. Given the dimensionless expression (15), it is possible to determine the friction angle of the material from the ratio of two hardness measurements:

$$\frac{H_1}{H_2} = \frac{\mathcal{H}_c(\varphi, \theta_1)}{\mathcal{H}_c(\varphi, \theta_2)} = \frac{\delta'(\varphi, \theta_1)}{\delta'(\varphi, \theta_2)}. \tag{25}$$

Fig. 7 displays the hardness ratio for the Berkovich and Corner–Cube indenters ($\theta_1 = \theta_B; \theta_2 = \theta_{CC}$) as a function of the friction angle in the interval $\varphi \in [5^\circ, 30^\circ]$. The figure confirms that there is a unique relation between the hardness ratio and the friction angle, which provides a means of assessing φ from the difference in hardness between a Berkovich indentation test and a Cube Corner indentation test. While small for very small friction angles, the hardness ratio becomes significant for greater friction angles, for which the ratio appears to increase almost linearly with the friction angle in the interval considered. Once the friction angle is determined, it is possible to determine the cohesion from the H/c curves displayed in Fig. 6.

4. Validation for a model cohesive-frictional material: bulk metallic glass

This Section deals with the validation of the proposed dual conical indentation technique for a ‘model’ material, bulk metallic glass, which has been recently found to exhibit a cohesive-frictional behavior from the scale of its atoms (Schuh and Lund, 2003) to the microscale of indentation analysis (Vaidyanathan et al., 2001) and the macroscale of laboratory test specimens (Donovan, 1989; Lu and Ravichandran, 2003). Furthermore, bulk metallic glass shows an almost elastic-perfectly plastic behavior in uniaxial compression/tension, with almost no strain hardening. This makes the application of a yield design approach even more appealing for this model material.

The material investigated is an as-cast fully amorphous $Zr_{41.2}Ti_{13.8}Cu_{12.5}Ni_{10}Be_{22.5}$ bulk metallic glass (which goes by the commercial name Vitreloy 1TM), manufactured by Howmet Corporation, Greenwich, CT. It is the same Zr-based material composition investigated by Lu and Ravichandran (2003) and Vaidyanathan et al. (2001). The elastic properties of this material are well known by now, from both ultrasonic measurements (Lu and Ravichandran, 2003) and microindentation tests (Vaidyanathan et al., 2001):

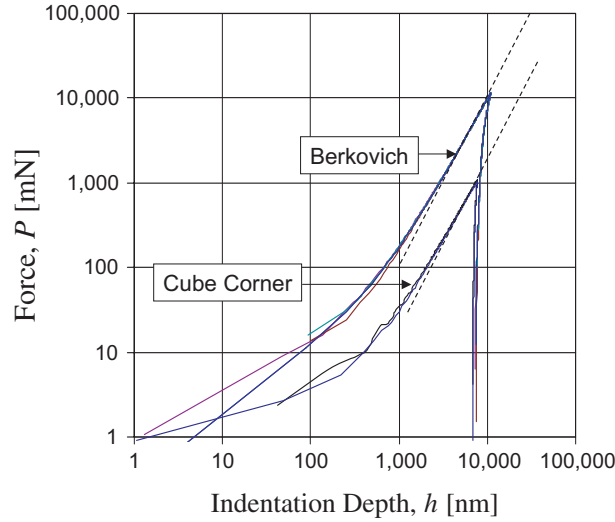


Fig. 8. Characteristic P - h curves for Berkovich and Cube Corner indentation in metallic glass. Note the log-log scale showing the repeatability of the test procedure and the $P \propto h^m$ scaling, which for $h \geq 4 \mu\text{m}$ is close to $m = 2$ (dashed lines) consistent with dimensionless relation (3a).

Young's modulus $E = 96 \text{ GPa}$, Poisson's ratio $\nu = 0.36$. An indentation campaign with a Berkovich indenter and a Cube corner indenter was performed. The indentations tests were load controlled at a constant rate of 300 mN/s . Fig. 8 displays characteristic P - h curves for the two indenter geometries. Indentation size effects were found to be negligible for indentation depth larger than $4 \mu\text{m}$, which is why we base our validation for maximum indentation depths of roughly $10 \mu\text{m}$, for which the dimensionless relations (2), (3a), (3b), (4) apply. In a traditional fashion, the projected contact area was measured from ESEM and AFM images of five residual impression left after complete unloading (Fig. 9), and the mean value (\pm accuracy of surface measurements) was taken to determine the hardness from its definition (1):

$$H_B = 5.42 \pm 0.03 \text{ GPa} ; \quad H_{CC} = 5.13 \pm 0.22 \text{ GPa}. \quad (26)$$

These values yield a hardness ratio (calculated from the meanvalues) of $H_B/H_{CC} = 1.057$, which we use in Fig. 7 to obtain the friction angle:

$$\frac{H_B}{H_{CC}} = 1.057 \pm 0.04 \Rightarrow \varphi = 7.3^\circ \pm 2.7^\circ. \quad (27)$$

Furthermore, use of the friction angle in Fig. 6 (resp. in Eq. (24)) yields the H_B/c and H_{CC}/c ratio. Since the hardness values (26) are known, we solve for the cohesion:

$$\tan \varphi = 0.13 \Rightarrow \left\{ \begin{array}{l} H_B/c = 7.15 \\ H_{CC}/c = 6.78 \end{array} \right\} \Rightarrow c = 760 \pm 30 \text{ MPa}. \quad (28)$$

In a last step, we need to verify the yield design assumption $(C_{ijkl}/c)^{-1} \rightarrow 0$, which reduces here to $c/E = 8 \times 10^{-3} \ll 1$. The fact that c/E is two orders of magnitude smaller than $\tan \varphi$ justifies a posteriori the use of our yield design solution for the extraction of the cohesion and friction angle.

Finally, the friction angle we obtain agrees remarkably well with the one obtained by Vaidyanathan et al. (2001) from extensive 3-D finite element back calculation of Berkovich indentation P - h curves ($\alpha = \tan \varphi = 0.13; Y_c = 1,900 \text{ MPa}$ in Vaidyanathan et al., 2001), and with values obtained by molecular statics simulations of Zr- and Cu-based metallic glasses by Schuh and Lund (2003); $\tan \varphi = 0.123 \pm$

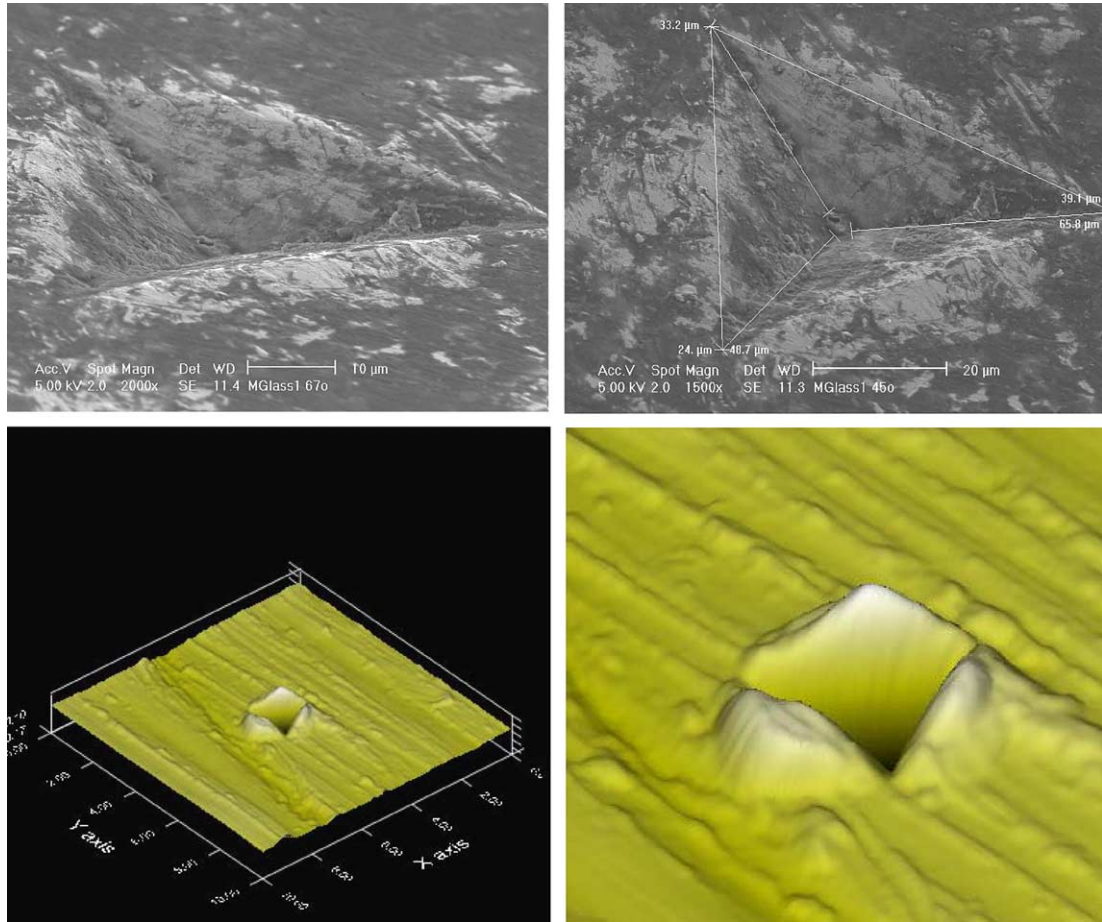


Fig. 9. Traditional measurements of projected contact area from residual impression after unloading: ESEM images of Berkovich indenter (TOP); AFM topographic images of Cube Corner imprint on metallic glass. The projected contact areas as seen through the microscope on a plan-view were measured using straight line measurements. The accuracy of the length measurements was on the order of $0.1 \mu\text{m}$, which translates into an accuracy of $10 \mu\text{m}^2$ in the area calculations.

0.004. The obtained friction coefficient and cohesion values also compare very well with the values Lu and Ravichandran reported from a large series of multiaxial compression tests for the same Zr-based bulk material ($\beta = \tan \varphi = 0.17; c = 804 \text{ MPa}$ in Lu and Ravichandran, 2003), and are on the same order of the macroscopic values reported by Donovan (1989) for Pd-based metallic glass ($\text{Pd}_{40}\text{Ni}_{40}\text{P}_{20}$) from uniaxial compression, plane-strain compression, plane-strain tension and shear tests ($\tan \varphi = 0.113 \pm 0.03; c = 795 \pm 25 \text{ MPa}$). The proposed dual indentation method which requires only two hardness measurements, complements these approaches and confirms (if need still be) that bulk metallic glasses are cohesive-frictional materials of the Mohr–Coulomb type.

5. Discussion

The dual indentation method we here propose is highly reductionist: it is based on the geometrical self-similarity of the conical indentation test and on yield design assumptions, reducing the number of param-

eters governing the hardness-to-cohesion ratio to two: the friction angle φ and the cone half-angle θ . In this reduced $(H/c, \varphi, \theta)$ invariant space, it is possible to ensure the uniqueness of the inverse analysis and extract the strength properties of cohesive-frictional materials. This method has several advantages, but also restrictions, compared to other inverse analysis methods:

1. The main advantage of the method is its ease of utilization: Compared to advanced finite element elastoplastic backanalysis of indentation curves, the method requires as input only two hardness values corresponding to two indenter geometries (cone half-angle θ). By means of fundamental dimensionless relations for the hardness-to-cohesion ratio, we find that the hardness-to-hardness ratio is a unique function of the friction angle, which ensures the uniqueness of the reverse problem. We demonstrated this method for two indenters commonly employed in instrumented indentation, Berkovich and Corner Cube indenter assimilated to cones of different apex angles. Of course, the same method could be employed with any other apex angle, and the method is the more efficient the higher the H/c -contrast between two apex angles for a given friction angle. We should also note that such a contrast is not achieved by spherical indentation of different sphere radius-to-indentation depth ratios, R/h , which replaces the tip half-angle in the dimensionless relation (6), ie. $H/c = \mathcal{H}_s(\varphi, R/h)$, making the conical indentation test the most efficient way to extract cohesion and friction angle from hardness measurements. We come to this conclusion from lower and upper bound H/c -solutions for spherical indentation which we obtained with our optimization algorithms. Not surprisingly, we also found that it is not possible to extract the friction angle from the hardness ratio of two indenter geometries that do not belong to the same family of self-similar indenter shapes (for a review of the conditions under which frictionless Hertz type contact problems possess classical self-similarity, see Borodich et al., 2003); for instance from a combination of conical and spherical indentation; entailing the non-uniqueness of the reverse problem (for details, see Ganneau and Ulm, 2004). This emphasizes that the geometrical self-similarity is a necessary condition for the uniqueness of the proposed inverse procedure.
2. The main analytical tools we employ in our method are fundamental $H/c = \mathcal{H}_c(\varphi, \theta)$ relations which we developed from a novel computational implementation of the limit theorems in axi-symmetrical conditions. One restriction of our approach relates to the assumption of the normality rule (or principle of maximum plastic work), which is at the very basis of the existence of the limit theorems of yield design, and which cannot capture an eventually non-associated flow behavior of the plastically deforming matter. From the perspective of dimensional analysis, the consideration of a non-associated flow rule adds one additional independent quantity, the dilatation angle, to the set of parameters in relations (2); but cannot be handled by the proposed yield design solution procedure in which the dilatation angle equals the friction angle. For such materials, advanced finite element simulations are required. In this case, the proposed method can be used to determine initial values of the cohesion and friction angle for the iterative backanalysis. A similar remark can be made for contact friction (which has been investigated for cohesive materials by Chitkara and Butt, 1992) and strain hardening effects, which we ignore in our yield design solutions. These effects appear to be negligible in the case of our ‘model’ material, since the diamond-metal contact friction is relatively low, and since metallic glass shows almost no strain hardening. Both effects may gain some importance for other materials, and may become significant particularly for small indenter angles for which pile-up occurs.
3. It could also be (and has been) argued that yield design approaches cannot capture piling-up or sinking-in phenomena, as yield design evaluates the dissipation capacity of a materials system for a fixed geometry. Indeed, in our upper-bound simulations, we assumed the surface surrounding the indenter to be flat, which is far from what is observed on topographic images in indentation tests particularly for very sharp indenters like the Corner Cube (see Fig. 9). However, compared to the material bulk volume that contributes to the overall dissipation capacity (see Fig. 5), the additional contribution of the pile-up material volume is expected to be of second-order in the evaluation (8) of the maximum dissipation

the material system can afford. Of course, the piling-up or sinking-in phenomena cannot be neglected in the evaluation of the hardness values from its definition (1), which are the input to our method. Hence, like all indentation procedures, the successful determination of the strength properties from the two indentation tests relies on the determination of the correct projected contact area. This is not an easy task: in the validation of our method for metallic glass, we measured the contact area by direct measurement of the residual hardness impression after a complete unloading. For practical reasons, however, some means other than direct observation of the hardness impressions is needed. Several methods that circumvent the necessity to measure the contact area have been proposed (for a recent review see Oliver and Pharr, 2004), and have been validated primarily for blunt and spherical indenter. It is expected that similar methods will become soon available also for very sharp indenters and cohesive-frictional materials having a pronounced plastic dilating behavior. In fact, from visual inspections, we found out that the Berkovich indenter has a contact-height-to-indentation depth ratio of $h_c/h = \sqrt{\Pi_\beta(\varphi, \theta_B)}/\pi \cot \theta_B = 0.85$ (see Fig. 1 and relation (3b)), which is well captured by existing indirect methods (Oliver and Pharr, 1992); while $h_c/h = \sqrt{\Pi_\beta(\varphi, \theta_{CC})}/\pi \cot \theta_{CC} = 1.17$ for the Cube Corner indenter on metallic glass, which is not covered by such methods. Progress on this front is expected to complete our developments in the close future.

Acknowledgements

This research was supported by a Presidential Fellowship of F. Ganneau at MIT, and discretionary funds provided by the Reed Fund of the School of Engineering and the Schoettler Scholarship Fund of the Department of Civil & Environmental Engineering at M.I.T. Additional industrial support was provided by Chevron Texaco, whose financial support is gratefully acknowledged. The indentation tests were carried out in the Nanolab@MIT facilities, directed by Alan Schwartzman and supervised by Prof. Krystyn Van Vliet from MIT's Department of Materials Science and Engineering. The continuous support of the Nanolab@MIT team is also gratefully acknowledged. The meshes composed of triangles interfaced by discontinuity elements were generated using a commercial finite-element package, CESAR-LCPC. Finally, we are grateful for fruitful comments and suggestions from Prof. J. Salençon (Ecole Polytechnique, France), Dr. Dao and Prof. C.A. Schuh (both M.I.T.).

References

- Anderheggen, E., Knopfel, H., 1972. Finite element limit analysis using linear programming. *Int. J. Solids Struct.* 8, 1413–1431.
- Bathe, K.J., 1996. *Finite Element Procedures*. Prentice Hall, Upper Saddle River, NJ.
- Bishop, J.F.W., 1953. On the complete solution to problems of deformation of a plastic rigid material. *J. Mech. Phys. Solids* 2 (1), 43–53.
- Brinell, J.A., 1901. In: *Congres international des methodes d'essai des materiaux de construction*. Vol. 2, Paris, 83–94.
- Borodich, F.M., Keer, L.M., Korach, C.S., 2003. Analytical study of fundamental nanoindentation test relations for indenters of non-ideal shapes. *Nanotechnology* 14, 803–808.
- Borodich, F.M., Keer, L.M., 2004. Contact problems and depth-sensing nanoindentation for frictionless and frictional boundary conditions. *Int. J. Solids Struct.* 41, 2479–2499.
- Bottero, A., Negre, R., Pastor, J., Turgeman, S., 1980. Finite element method and limit analysis theory for soil mechanics problems. *Comput. Meth. Appl. Mech. Engng.* 22, 131–149.
- Bucaille, J.L., Stauss, S., Felder, E., Michler, J., 2003. Determination of plastic properties of metals by instrumented indentation using different sharp indenters. *Acta Mater.* 51, 1663–1678.
- Cheng, Y.-T., Cheng, C.-M., 2004. Scaling, dimensional analysis, and indentation measurements. *Mater. Sci. Eng.* R44, 91–149.
- Chitkara, N.R., Butt, M.A., 1992. Numerical Construction of axisymmetric slip-line fields for indentation of thick blocks by rigid conical indenters and friction at the tool-metal interface. *Int. J. Mech. Sci.* 34 (11), 849–862.

- Chollacoop, N., Dao, M., Suresh, S., 2003. Depth-sensing instrumented indentation with dual sharp indenters. *Acta Mater.* 51, 3713–3729.
- Constantinides, G., Ulm, F.-J., Van Vliet, K., 2003. On the use of nanoindentation for cementitious materials. *Mater. Struct.* 36, 191–196.
- DiCarlo, A., Yang, H.T.Y., Chandrasekar, S., 2003. Semi-inverse method for predicting stress–strain relationship from cone indentations. *J. Mater. Res.* 18 (9), 2068–2078.
- Donovan, P.E., 1989. A yield criterion for Pd₄₀Ni₄₀P₂₀ metallic glass. *Acta Metall.* 37, 445–456.
- Fremont, M., Salençon, J., 1973. Limit analysis by finite element methods. In: Palmer, A.C., (Ed.), *Proc. Symp. on Role of plasticity in soil mech.* Cambridge, UK.
- Futakawa, M., Wakui, T., Tanabe, Y., Ioka, I., 2001. Identification of the constitutive equation by the indentation technique using plural indenters with different apex angles. *J. Mater. Res.* 16 (8), 2283–2292.
- Ganneau, F., Ulm, F.-J., 2004. From nanohardness to strength properties of cohesive-frictional materials. Application to shale materials. MIT-CEE Res. Rep. 04-01 (MSc. Dissertation), Cambridge, MA.
- Hopkins, H.G., Cox, A.D., Eason, G., 1961. Axially symmetric plastic deformation in soils. *Philos. Trans. Roy. Soc.* A264, 1–45.
- Houlsby, G.T., Wroth, C.P., 1982. Determination of undrained strengths by cone penetration tests. In: *Proc. 2nd European Symposium on Penetration Testing*, Amsterdam, NL.
- Igarashi, S., Bentur, A., Mindess, S., 1996. Characterization of the microstructure and strength of cement paste by microhardness testing. *Adv. Cement Res.* 8 (30), 877–892.
- Johnson, K.L., 1985. *Contact Mechanics*, 9th printing. Cambridge University Press, Cambridge, UK.
- Kholmyansky, M., Kogan, E., Kovler, K., 1994. On the hardness determination of fine-grained concrete. *Mater. Struct.* 27, 584–587.
- Lockett, F.J., 1963. Indentation of a rigid/plastic material by a conical indenter. *J. Mech. Phys. Solids* 11, 345.
- Lu, J., Ravichandran, G., 2003. Pressure-dependent flow behavior of Zr_{41.2}Ti_{13.8}Cu_{12.5}Ni₁₀Be_{22.5} bulk metallic glass. *J. Mater. Res.* 18 (9), 2039–2049.
- Lyamin, A.V., Sloan, S.W., 2002a. Lower bound limit analysis using non-linear programming. *Int. J. Numer. Anal. Meth. Geomech.* 26, 181–216.
- Lyamin, A.V., Sloan, S.W., 2002b. Upper bound limit analysis using linear finite elements and non-linear programming. *Int. J. Numer. Meth. Engng.* 55, 573–611.
- Lysmer, L., 1970. Limit analysis of plane problems in soil mechanics. *ASCE J. Soil Mech. Found. Div.* 96, 1311–1334.
- Min, L., Wei-min, C., Nai-gang, L., Ling-Dong, W., 2004. A numerical study of indentation using indenters of different geometry. *J. Mater. Res.* 19 (1), 73–78.
- Oliver, W.C., Pharr, G.M., 1992. An Improved Technique for Determining Hardness and Elastic Modulus Using Load and Displacement Sensing Indentation Experiments. *J. Mater. Res.* 7 (6), 1564–1583.
- Oliver, W.C., Pharr, G.M., 2004. Measurement of hardness and elastic modulus by instrumented indentation: Advances in understanding and refinements to methodology. *J. Mater. Res.* 19 (1), 3–20.
- Pastor, J., 1976. Application de l'analyse limite a l'etude de la stabilite des pentes et des talus. Ph.D. dissertation, USMG, Grenoble, France.
- Pastor, J., Turgeman, S., 1976. Mise en oeuvre numerique des methodes de l'analyse limite pour les materiaux de Von Mises et de Coulomb standards en deformation plane. *Mech. Res. Comm.* 3, 469–476.
- Salençon, J., 1983. *Calcul à la rupture et analyse limite*. Presses de l'Ecole nationale des ponts et chaussées, Paris, France.
- Salençon, J., Matar, M., 1982. Capacité portante des fondations superficielles circulaires. *J. Mécanique Théorique et Appliquée* 1 (2), 237–267, Available in English: *Foundation Engineering*, Vol. 1, Soil properties-foundation design and construction, Presse de l'Ecole Nationale des Ponts et Chaussées, France.
- Schuh, C.A., Nieh, T.G., 2004. A survey of instrumented indentation studies on metallic glasses. *J. Mater. Res.* 19 (1), 47–57.
- Schuh, C.A., Lund, A.C., 2003. Atomistic basis for the plastic yield criterion of metallic glass. *Nature Materials* 2, 449–452.
- Sloan, S.W., 1988a. Lower bound limit analysis using finite elements and linear programming. *Int. J. Numer. Anal. Meth. Geomech.* 12, 61–77.
- Sloan, S.W., A steepest edge active set algorithm for solving sparse linear programming problems. *Int. J. Numer. Anal. Meth. Geomech.* 12, 2671–2685.
- Sloan, S.W., Kleeman, P.W., 1995. Upper bound limit analysis with discontinuous velocity fields. *Comput. Meth. Appl. Mech. Engng.* 127, 293–314.
- Swaddiwudhipong, S., Tho, K.K., Liu, Z.S., Zeng, K., 2005. Material characterization based on dual indenters. *Int. J. Solids Struct.* 42, 69–83.
- Tabor, D., 1948. A simple theory of static and dynamic hardness. *Proc. Roy. Soc.* A192, 247 (cited from Johnson, 1985).
- Tabor, D., 1951. *The hardness of metals*. Oxford classical texts in the physical sciences. Edition 2000, UK.
- Turgeman, S., 1976. Etude des fondations sollicitées a l'arrachement par la theorie de l'analyse limite. Ph.D. dissertation, USMG, Grenoble, France.

- Vaidyanathan, R., Dao, M., Ravichandran, G., Suresh, S., 2001. Study of mechanical deformation in bulk metallic glass through instrumented indentation. *Acta mater.* 49, 3781–3789.
- Williams, S.R., 1942. *Hardness and Hardness Measurements*. American Society of Metals, Cleveland, Ohio.